Molecular Layer Deposition of Hybrid Organic−Inorganic Alucone Polymer Films Using a Three-Step ABC Reaction Sequence

Byunghoon Yoon,[†] Dragos Seghete,[†] Andrew S. Cavanagh,[‡,§] and Steven M. George*,[†,§,||]

[†]*Department of Chemistry and Biochemistry,* [‡]*Department of Physics,* [§]*DARPA Center for Integrated Micro/Nano-Electromechanical Transducers (iMINT),* [||]*Department of Chemical and Biochemical Engineering, and University of Colorado at Boulder, Colorado 80309*

Received May 14, 2009. Revised Manuscript Received September 25, 2009

Thin film growth using molecular layer deposition (MLD) or atomic layer deposition (ALD) is based on sequential, self-limiting surface reactions. In this work, MLD is used to grow a hybrid organic−inorganic polymer film based on a three-step ABC reaction sequence using trimethylaluminum (TMA), ethanolamine (EA), and maleic anhydride (MA) as the reactants. This three-step ABC sequence avoids the use of homobifunctional organic precursors by employing a homotrifunctional inorganic reactant (TMA), a heterobifunctional organic reactant (EA), and a ring-opening organic reactant (MA). The resulting hybrid organic−inorganic polymer film is an alucone with an approximate formula of $(-AlCH_3-OCH_2CH_2NH-C(O)CHCHCOO-)_n$. The growth of this ABC alucone film was monitored using in situ Fourier transform infrared (FTIR) measurements at 90−170 °C. The three sequential surface reactions displayed self-limiting growth. The FTIR difference spectra monitored the absorbance from the surface species during the three surface reactions. The gain and loss of absorbance helped to determine the reaction mechanism for the ABC alucone film growth. Transmission electron microscope (TEM) measurements on ZrO_2 nanoparticles also displayed the growth of very conformal ABC alucone films. The ABC alucone growth per cycle was also measured on Si wafers using X-ray reflectivity. ABC alucone growth rates were temperature dependent and varied from 24 Å per cycle at 90 °C to 4.0 Å per cycle at 170 °C. X-ray photoelectron spectroscopy also determined the composition of the ABC alucone films. The robust and efficient growth of the ABC alucone hybrid organic−inorganic films may be useful in applications requiring flexible or sacrificial films.

I. Introduction

Atomic layer deposition (ALD) is a growth technique for inorganic thin films based on sequential, self-limiting surface reactions.[1−4] Molecular layer deposition (MLD) is a related method for the growth of organic thin films that also relies on sequential, self-limiting surface reactions.[5−7] MLD was originally developed for a variety of organic polymers such as polyamides[5,8,9] and polyimides.[7,10] The reactants in inorganic ALD and organic MLD processes can be combined to grow hybrid organic−inorganic thin films.[6,11,12] One of the first demonstrations of ALD/MLD hybrid films was the growth of aluminum alkoxides known as alucones[13] using trimethylaluminum (TMA) and ethylene glycol (EG).[11] The number of possible combinations using ALD and MLD reactants is very extensive.[14] The growth of hybrid organic−inorganic thin films was recently expanded to the growth of "zincone" films using diethylzinc (DEZ) and EG.[15,16]

Although some ternary compounds can be grown by ALD, most of the ALD and MLD procedures developed to date are based on only two reactants in an AB binary reaction sequence. The use of organic precursors in MLD opens up the immense variety of possible reactions from organic chemistry.[6] Likewise, the number of possible reactions that can be used in MLD is greatly enlarged if the AB binary reaction sequence is extended to an ABC

(1) George, S. M.; Ott, A. W.; Klaus, J. W. *J. Phys. Chem.* **1996,** *100,* 13121.
(2) Puurunen, R. L. *J. Appl. Phys.* **2005,** *97,* 121301.
(3) Ritala, M.; Leskela, M. Atomic Layer Deposition. In *Handbook of Thin Film Materials;* Nalwa, H. S., Ed.; Academic Press: San Diego, CA, 2001; Vol. *1.*
(4) Suntola, T. *Thin Solid Films* **1992,** *216,* 84.
(5) Du, Y.; George, S. M. *J. Phys. Chem. C.* **2007,** *111,* 8509.
(6) George, S. M.; Yoon, B.; Dameron, A. A. *Acc. Chem. Res.* **2009,** *42,* 498.
(7) Yoshimura, T.; Tatsuura, S.; Sotoyama, W. *Appl. Phys. Lett.* **1991,** *59,* 482.
(8) Adamcyzk, N. M.; Dameron, A. A.; George, S. M. *Langmuir* **2008,** *24,* 2081.
(9) Shao, H. I.; Umemoto, S.; Kikutani, T.; Okui, N. *Polymer* **1997,** *38,* 459.
(10) Putkonen, M.; Harjuoja, J.; Sajavaara, T.; Niinisto, L. *J. Mater. Chem.* **2006,** *17,* 664.
(11) Dameron, A. A.; Seghete, D.; Burton, B. B.; Davidson, S. D.; Cavanagh, A. S.; Bertand, J. A.; George, S. M. *Chem. Mater.* **2008,** *20,* 3315.

(12) Nilsen, O.; Klepper, K. B.; Nielson, H. O.; Fjellvag, H. *ECS Trans.* **2008,** *16,* 3.
(13) McMahon, C. N.; Alemany, L.; Callender, R. L.; Bott, S. G.; Barron, A. R. *Chem. Mater.* **1999,** *11,* 3181.
(14) Nilsen, O.; Fjellvag, H. Thin Films Prepared with Gas Phase Deposition Technique. Patent WO 2006/071126 A1, July 6, **2006.**
(15) Peng, Q.; Gong, B.; VanGundy, R. M.; Parsons, G. N. *Chem. Mater.* **2009,** *21,* 820.
(16) Yoon, B.; O'Patchen, J. L.; Seghete, D.; Cavanagh, A. S.; George, S. M. *Chem. Vap. Deposit.* **2009,** *15,* 112.

Report Documentation Page

Form Approved
OMB No. 0704-0188

Public reporting burden for the collection of information is estimated to average 1 hour per response, including the time for reviewing instructions, searching existing data sources, gathering and maintaining the data needed, and completing and reviewing the collection of information. Send comments regarding this burden estimate or any other aspect of this collection of information, including suggestions for reducing this burden, to Washington Headquarters Services, Directorate for Information Operations and Reports, 1215 Jefferson Davis Highway, Suite 1204, Arlington VA 22202-4302. Respondents should be aware that notwithstanding any other provision of law, no person shall be subject to a penalty for failing to comply with a collection of information if it does not display a currently valid OMB control number.

1. REPORT DATE **2009**	2. REPORT TYPE	3. DATES COVERED **00-00-2009 to 00-00-2009**

4. TITLE AND SUBTITLE	5a. CONTRACT NUMBER
Molecular Layer Deposition of Hybrid Organic -- Inorganic Alucone Polymer Films Using a Three-Step ABC Reaction Sequence	5b. GRANT NUMBER
	5c. PROGRAM ELEMENT NUMBER
6. AUTHOR(S)	5d. PROJECT NUMBER
	5e. TASK NUMBER
	5f. WORK UNIT NUMBER

7. PERFORMING ORGANIZATION NAME(S) AND ADDRESS(ES) **Department of Chemistry and Biochemistry,University of Colorado,Boulder,CO,80309**	8. PERFORMING ORGANIZATION REPORT NUMBER

9. SPONSORING/MONITORING AGENCY NAME(S) AND ADDRESS(ES)	10. SPONSOR/MONITOR'S ACRONYM(S)
	11. SPONSOR/MONITOR'S REPORT NUMBER(S)

12. DISTRIBUTION/AVAILABILITY STATEMENT
Approved for public release; distribution unlimited

13. SUPPLEMENTARY NOTES

14. ABSTRACT

15. SUBJECT TERMS

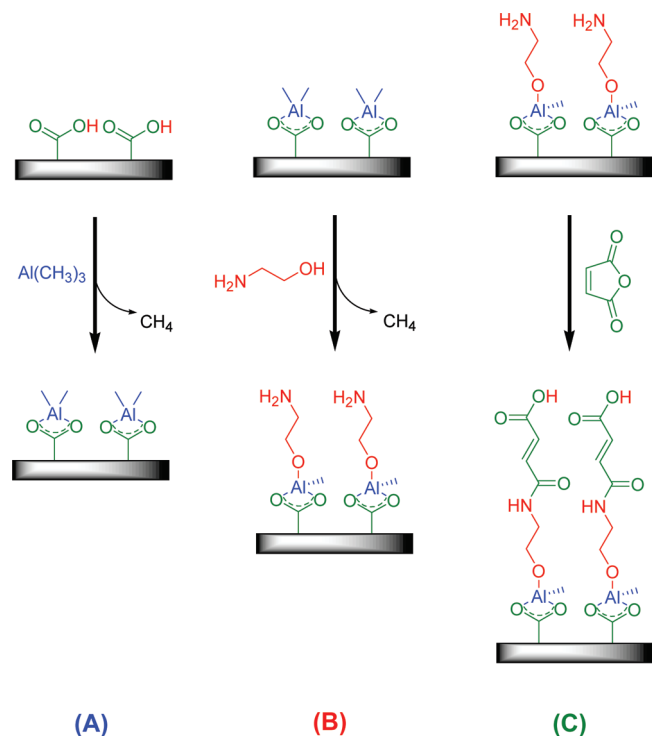| 16. SECURITY CLASSIFICATION OF:			17. LIMITATION OF ABSTRACT	18. NUMBER OF PAGES	19a. NAME OF RESPONSIBLE PERSON
a. REPORT **unclassified**	b. ABSTRACT **unclassified**	c. THIS PAGE **unclassified**	**Same as Report (SAR)**	**10**	

Figure 1. Schematic of three-step reaction sequence for ABC alucone growth using (A) trimethylaluminum (TMA), (B) ethanolamine (EA), and (C) maleic anhydride (MA).
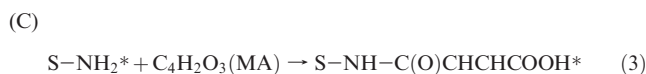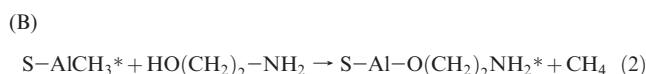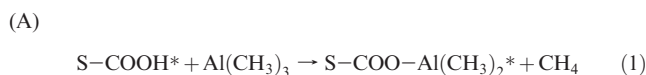
ternary reaction sequence. The third reactant can optimize the MLD process by providing an additional surface functional group that may facilitate the overall ABC reaction sequence. The extra reactant also increases the ability to incorporate particular functionalities into the MLD film.

AB binary reaction sequences usually employ homobifunctional reactants such as EG in the TMA + EG alucone reaction.[11] One of the major problems with AB binary reaction sequences is "double" reactions between the homobifunctional reactant and the surface species.[8,11] These double reactions can limit the number of active surface sites and reduce the growth per cycle and lead to varying growth rates. Double reactions have been observed or implicated in the MLD of poly(*p*-phenylene terephthalamide) using terephthaloyl chloride and *p*-phenylenediamine,[8] alucone using TMA and EG,[11] and zincone using DEZ and EG.[16] One of the benefits of the ABC ternary reaction sequence is that new reactants can be employed that avoid the possibility of double reactions that occur with homobifunctional reactants.

New precursors such as heterobifunctional and ring-opening reactants can be defined in the ABC ternary reaction sequence.[6] One end of the heterobifunctional reactant may react preferentially to avoid the double reaction. Likewise, ring-opening reactants may react and yield a new functional group upon ring-opening that does not react with the initial surface species. These new precursors may be able to achieve much higher growth per cycle during MLD because double reactions have not eliminated active surface species. In spite of their

potential advantages, there have been no detailed reports of three-step ABC reaction sequences for the MLD of organic or hybrid organic—inorganic polymer films.[6]

In this paper, the MLD of a hybrid organic—inorganic polymers is reported using a three-step ABC ternary reaction sequence based on (1) TMA, a homomultifunctional inorganic precursor; (2) ethanolamine (EA), a heterobifunctional organic reactant, and (3) maleic anhydride (MA), a ring-opening organic reactant.[6] The proposed reaction sequence during this three-step MLD process is shown in Figure 1. The proposed surface reactions during the ABC alucone growth is

(A)

$$S{-}COOH^* + Al(CH_3)_3 \rightarrow S{-}COO{-}Al(CH_3)_2{}^* + CH_4 \quad (1)$$

(B)

$$S{-}AlCH_3^* + HO(CH_2)_2{-}NH_2 \rightarrow S{-}Al{-}O(CH_2)_2NH_2^* + CH_4 \quad (2)$$

(C)

$$S{-}NH_2^* + C_4H_2O_3(MA) \rightarrow S{-}NH{-}C(O)CHCHCOOH^* \quad (3)$$

The asterisks indicate the surface species and S denotes the substrate with the reaction products from the previous reactions.

In this ABC reaction sequence, TMA reacts with carboxylic groups in reaction A given by eq 1 to form $AlCH_3^*$ species. Subsequently, the $AlCH_3^*$ species react preferentially with the hydroxyl end of the EA reactant to form $AlOCH_2CH_2NH_2^*$ surface species in reaction B given by eq 2. MA then reacts with amine-terminated surface functional groups to reform carboxylic groups through a ring-opening reaction in reaction C given by eq 3. The three-step ABC sequence is then repeated by exposure to TMA, EA, and MA to grow the ABC alucone film.

To confirm the thin film growth process and measure the growth rates, a variety of techniques are employed in these studies. In situ transmission Fourier transform infrared (FTIR) investigations are used to monitor the surface reactions during the TMA, EA, and MA sequential exposures. Transmission electron microscopy (TEM) images are utilized to measure the film thickness and film conformality on nanoparticles coated by this ABC ternary reaction sequence. X-ray reflectivity scans are also employed to measure the film thickness of the ABC alucone thin film on Si wafers versus number of MLD cycles. These techniques establish this new three-step ABC reaction sequence for hybrid organic—inorganic polymers.

II. Experimental Section

The studies were conducted in a viscous flow reactor equipped with an in situ FTIR spectrometer that has been described previously.[8,16] The organic and inorganic reactants were pumped by a liquid N_2 trap and a mechanical pump. The mechanical pump maintained a pressure of 0.70 Torr with a N_2

carrier gas flow of 100 sccm into the reactor. The N_2 carrier gas helped transport reactants into the reactor and remove reaction products from the reactor.

The in situ FTIR studies were performed with a Nicolet Nexus 870 FTIR spectrometer equipped with a liquid-N_2 cooled mercury−cadmium−telluride (MCT-B) infrared detector.[5,8,16] Spectra were collected with a mirror speed of 1.8 cm·s^{-1} and averaged over 100 scans using a resolution of 4 cm^{-1}. Transparent KBr windows supplied by International Crystal Laboratories were used to transmit the infrared beam through the reactor. The spectrometer setup was purged with dry and CO_2-free air delivered from a purge gas generator.

Transmission FTIR spectroscopy measurements on high surface area samples were used to monitor the absorbance from surface species with high signal-to-noise.[17] The high surface area samples were spherical zirconia (ZrO_2) nanoparticles with an average diameter of 25 nm. The nanoparticles were pressed into a stainless steel grid using methods described earlier.[17,18] The stainless steel grids supporting the ZrO_2 nanoparticles were obtained from Tech Etch. The ZrO_2 nanoparticles were obtained from Sigma-Aldrich.

The three-step alucone MLD growth was monitored at 90, 110, 130, 150, and 170 °C. The TMA, EA, and MA reactants were obtained from Sigma-Aldrich. The TMA source was held at room temperature. For the TMA reaction to reach completion, each TMA exposure consisted of a 1.0 s TMA dose at a partial pressure of 400 mTorr. The EA and MA reactants were maintained at 50 °C. For the EA and MA reactions to reach completion, each EA exposure was composed of five 1.0 s EA doses. Each EA dose produced a partial pressure of 35 mTorr. Each MA exposure consisted of a 1.0 s MA dose at a partial pressure of 110 mTorr. Purge time of 120, 120, and 120 s were used after each TMA, EA, and MA dose, respectively. One set of TMA, EA, and MA exposures defined one MLD cycle. The ABC alucone film growth reached steady state behavior after 4−5 MLD cycles.

The ex situ X-ray reflectivity (XRR) scans were acquired using a high resolution Bede D1 X-ray diffractometer from Bede Scientific. The X-ray diffractometer used a Cu X-ray tube. A collimator (Osmic Max-Flux) and a channel cut crystal restricted the Cu Kα radiation to Cu Kα$_1$ radiation at 1.540 Å. A filament current of 40 mA and a voltage of 40 kV were used for the XRR measurements. The thicknesses of the alucone ABC films on the thin native oxide on Si wafers were extracted using the REFS data fitting software from Bede Scientific. The ABC alucone films analyzed by XRR for thickness, roughness, and density were deposited on boron doped *p*-type silicon wafers purchased from Silicon Valley Microelectronics, Inc.

The X-ray photoelectron spectroscopy (XPS) results were obtained using a Phi 5600 photoelectron spectrometer with monochromatic Al Kα source at 1486.6 eV (12.5 mA, 12 kV) with a pressure of 2×10^{-10} Torr. The binding energies were referenced to the adventitious C 1s peak at 285 eV for all spectra. Elemental composition was determined from the peak areas for C 1s, N 1s, O 1s and 2s, and Al 2s and 2p. The TEM analysis was performed using a Philips CM10 transmission electron microscope with an 80 kV beam energy. The MLD growth per cycle was determined by measuring the alucone ABC film thickness on the ZrO_2 nanoparticles and dividing by the number of MLD cycles.

Table 1. Assignment of Vibrational Peaks Observed during ABC Alucone MLD

frequency (cm^{-1})	assignment
3750−3050	OH
3160−3420	NH_2 stretch, EA
3044	$R_1=CH-R_2$ stretch, MA
2963	CH_2 antisymmetric stretch, EA
2927	CH_3 antisymmetric stretch, TMA
2898	CH_3 symmetric stretch, TMA
2872	CH_2 symmetric stretch, EA
1720	carboxylic acid C=O antisymmetric stretch, MA
1668	C=O stretch, MA
1638	Amide I C=O stretch, MA
1635	NH_2 scissoring, EA
1585	CO_2^- bidentate asymmetric stretch, TMA
1578	−C=C− stretch, MA
1540	*trans*-secondary amide II, O=CR−NR′−H, MA
1467	CO_2^- bidentate symmetric stretch, TMA
1446	C−C stretch, MA
1390	CH_2 scissoring, EA
1345	=C−H bending, MA
1310	CH_2 wagging, EA
1270	CH_2 twisting, EA
1205	CH_3 deformation, TMA
1080	C−O stretch, EA
975	R−HC=CH−R′ C=C *trans* wagging, MA
883	Al−O stretch, EA

III. Results and Discussion

A. Fourier Transform Infrared Spectroscopy. The ABC alucone growth based on TMA, EA, and MA reactants was studied using in situ transmission FTIR analysis for temperatures from 90 to 170 °C on the high surface area ZrO_2 nanoparticles. The in situ FTIR spectra were recorded after each reactant exposure. The vibrational assignments of the observed absorbance peaks between 800 and 4000 cm^{-1} are listed in Table 1. These vibrational features have been identified previously.[19]

Figure 2 displays the absolute FTIR spectra after consecutive TMA, EA, MA, and TMA exposures on the ZrO_2 nanoparticles at 150 °C. These FTIR spectra are all referenced to the KBr windows and have been displaced for clarity in presentation. Figure 2a shows the FTIR spectra of the hydroxylated ZrO_2 nanoparticles with a broad absorbance from O−H stretching vibrations at 2470−3810 cm^{-1} and bulk ZrO_2 absorption at <800 cm^{-1}. The O−H stretching vibrations are known to have a wide absorbance range on metal oxide surfaces.[20−22] After TMA exposure on the hydroxylated ZrO_2 substrate, Figure 2b shows the absorbance from C−H stretching vibrations at 2800−3000 cm^{-1} and from the methyl deformation of AlCH$_3$* species at 1205 cm^{-1}. Figure 2c then reveals the absorbance from C−O stretching vibrations, NH_2 scissoring modes, and primary N−H stretching vibrations at 1085, 1635, and 3160−3420 cm^{-1}, respectively, after EA exposure.

(17) Ferguson, J. D.; Weimer, A. W.; George, S. M. *Chem. Mater.* **2004**, *16*, 5602.
(18) Ballinger, T. H.; Wong, J. C. S.; Yates, J. T. *Langmuir* **1992**, *8*, 1676.
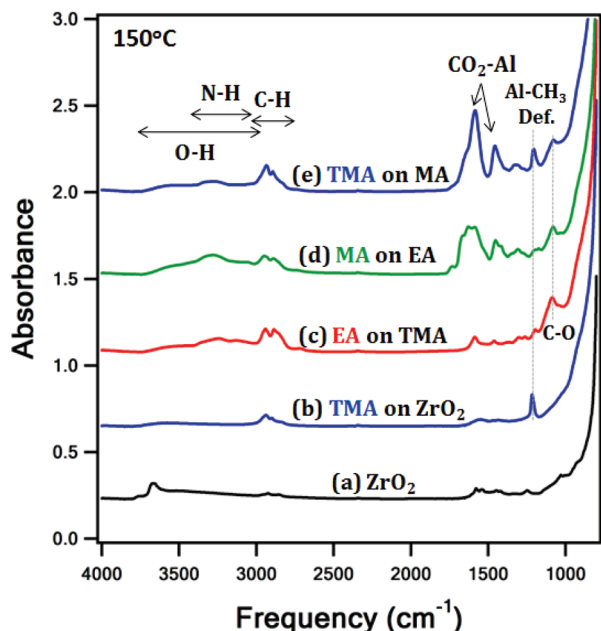
(19) Chalmers, J. M.; Griffiths, P. R. *Handbook of Vibrational Spectroscopy*; Wiley: New York, 2002.
(20) Dillon, A. C.; Ott, A. W.; Way, J. D.; George, S. M. *Surf. Sci.* **1995**, *322*, 230.
(21) Ferguson, J. D.; Weimer, A. W.; George, S. M. *J. Vac. Sci. Technol. A* **2005**, *23*, 118.
(22) Ferguson, J. D.; Yoder, A. R.; Weimer, A. W.; George, S. M. *Appl. Surf. Sci.* **2004**, *226*, 393.

Figure 2. Absolute FTIR spectra (a) of initial ZrO_2 nanoparticles and (b) after initial TMA exposure on ZrO_2 nanoparticles. Absolute FTIR spectra after subsequent (c) EA exposure, (d) MA exposure, and (e) TMA exposure. The ABC alucone MLD was performed at 150 °C.
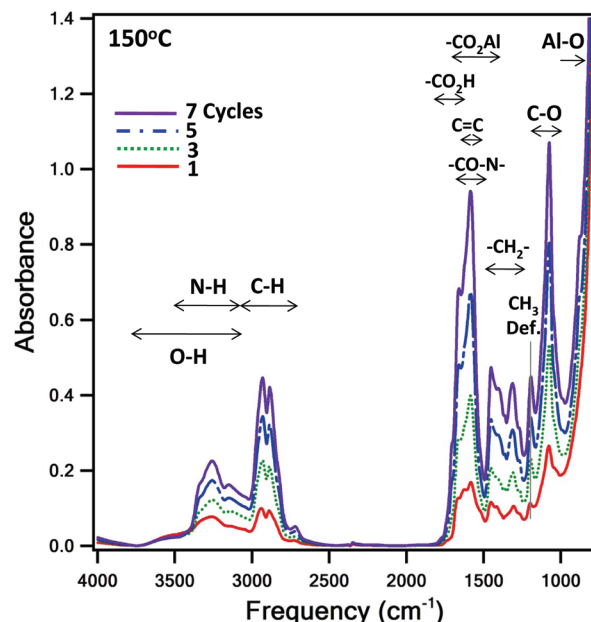

Figure 3. Progressive absolute FTIR spectra during ABC alucone MLD after 1, 3, 5, and 7 MLD cycles at 150 °C referenced with respect to the ZrO_2 nanoparticles. The absolute spectra were all recorded after the MA exposure.

During the MA exposure, the amine surface species react with MA to yield carboxylic surface species via a ring-opening reaction. Figure 2d shows the absorbance from the *trans*-secondary amide I and II vibrations and characteristic carboxylic acid peaks at 1638, 1540, and 1720 cm^{-1}, respectively. After the next TMA exposure, Figure 2e reveals that the carboxylic acid surface species react with TMA and yield characteristic peaks for an Al−carboxylic acid complex. Absorbance is observed from asymmetric and symmetric carboxylate ion stretching vibrations at 1585 and 1467 cm^{-1}. In addition, the absorbance from the methyl deformation of the AlCH$_3$* species is again observed at 1205 cm^{-1}.

The growth of the ABC alucone film after multiple MLD cycles on the ZrO_2 nanoparticles is also monitored by FTIR measurements. The FTIR spectra following the MA exposure after 1, 3, 5, and 7 MLD cycles at 150 °C are shown in Figure 3. The infrared absorbance grows progressively versus number of MLD cycles. The absorbances at 1085 and 1500−1730 cm^{-1} correspond with the C−O stretching vibrations and carbonyls stretching vibrations of amide and carboxylic acid functionalities. The other noticeable peaks are observed at 1190−1250, 1486−1550, and 2750−3000 cm^{-1}, corresponding with the methyl deformation of AlCH$_3$* species and C−N and C−H stretching vibrations, respectively. At high frequencies, absorbances are also observed at 3160−3420 and 3420−3750 cm^{-1}. These peaks are assigned to N−H and O−H stretching vibrations.

The integrated absorbances of the methyl deformation of AlCH$_3$* species at 1190−1250 cm^{-1}, N−H stretching vibrations at 3160−3420 cm^{-1}, and amide C=O and C−N stretching vibrations at 1486−1660 cm^{-1} can be used to monitor the self-limiting nature of the surface reactions

versus reactant exposure. The integrated absorbances for ABC alucone growth at 150 °C during the first several reaction cycles on the ZrO_2 nanoparticles are shown in Figure 4. The integrated absorbance from the methyl deformation mode of AlCH$_3$* species versus TMA exposure at 150 °C is shown in Figure 4a. The TMA exposure is defined by the number of TMA microdoses. Each TMA microdose was a 0.5 s exposure at 80 mTorr of partial pressure. Figure 4a indicates that the TMA reaction is self-limiting and reaches completion after 10 TMA microdoses.

The integrated absorbance from the N−H stretching vibrations versus EA exposure at 150 °C is shown in Figure 4b. The EA exposure is again defined by the number of EA microdoses. Each EA microdose was a 0.5 s exposure at 20 mTorr of partial pressure. Figure 4b indicates that the EA reaction is self-limiting and reaches completion after 12 EA microdoses. The loss of integrated absorbance from the methyl deformation mode of AlCH$_3$* species is also shown in Figure 4b. The reduction of this feature coincides with the gain of the integrated absorbance of the N−H stretching vibration. The AlCH$_3$* species is not completely removed by the EA exposure. Figure 4b indicates that ∼23% of the original integrated absorbance of the methyl deformation mode remains after 14 EA microdoses. In addition, the peak of this absorption shifts from 1205−1213 cm^{-1} after TMA exposure to 1190−1200 cm^{-1} after EA exposure.

The integrated absorbance from the amide C=O and C−N stretching vibration versus MA exposure at 150 °C is shown in Figure 4c. Each MA microdose was a 0.5 s exposure at 25 mTorr of partial pressure. Figure 4c indicates that the MA reaction is self-limiting and reaches completion after > 18 MA microdoses. The additional loss of integrated absorbance from the methyl deformation
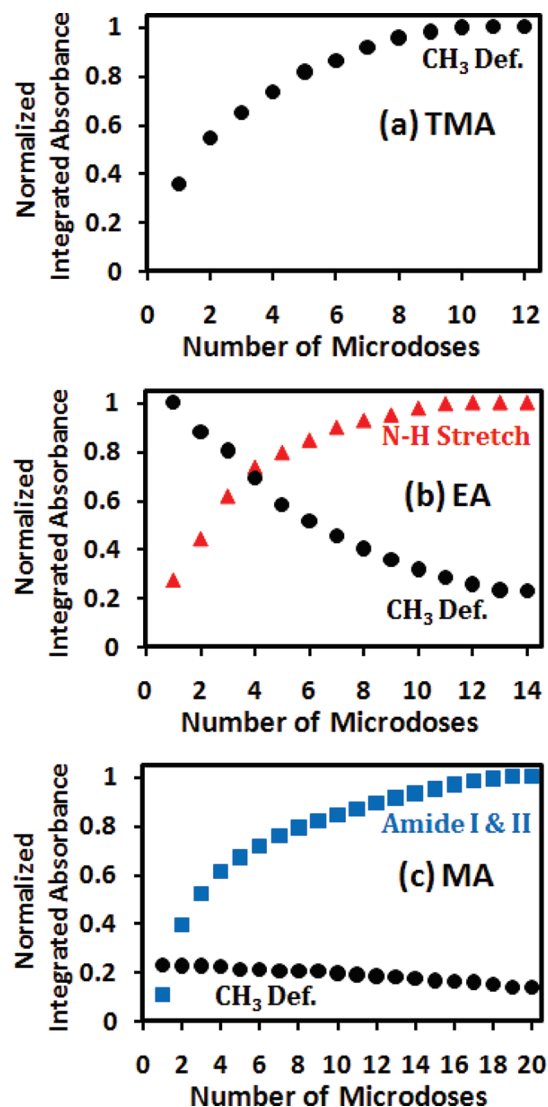
Figure 4. Self-limiting nature of surface reactions illustrated by integrated absorbances for (a) CH_3 deformation of $AlCH_3^*$ species versus TMA exposure, (b) N—H stretching vibrations and CH_3 deformation of $AlCH_3^*$ species versus EA exposure, and (c) amide I and amide II vibrations and CH_3 deformation of $AlCH_3^*$ species versus MA exposure. All exposures were performed at 150 °C.

Figure 5. FTIR difference spectra after TMA, EA, and MA exposures during ABC alucone MLD at 150 °C: (a) TMA−MA; (b) EA−TMA; and (c) MA−EA. The FTIR spectra after each reactant exposure are referenced with respect to the previous reactant exposure.

mode of $AlCH_3^*$ species is also displayed in Figure 4c. This feature is reduced to ∼14% of its original integrated absorbance after 20 MA microdoses. The peak of this absorption also remains at $1190-1200$ cm^{-1} after MA exposure.

The change of surface species during each reaction in the three-step ABC reaction sequence can be monitored by FTIR difference spectra. In the FTIR difference spectra, the added surface species appear as positive absorbance features and the removed surface species appear as negative absorbance features. The FTIR difference spectra after each reaction at 150 °C are shown in Figure 5. The spectra have again been displaced for clarity in presentation. Figure 5a, b, and c shows the FTIR difference spectra after TMA exposure onto an MA-saturated surface (TMA−MA), after EA exposure onto a TMA-saturated surface (EA−TMA), and after MA exposure onto an EA-saturated surface (MA−EA), respectively.
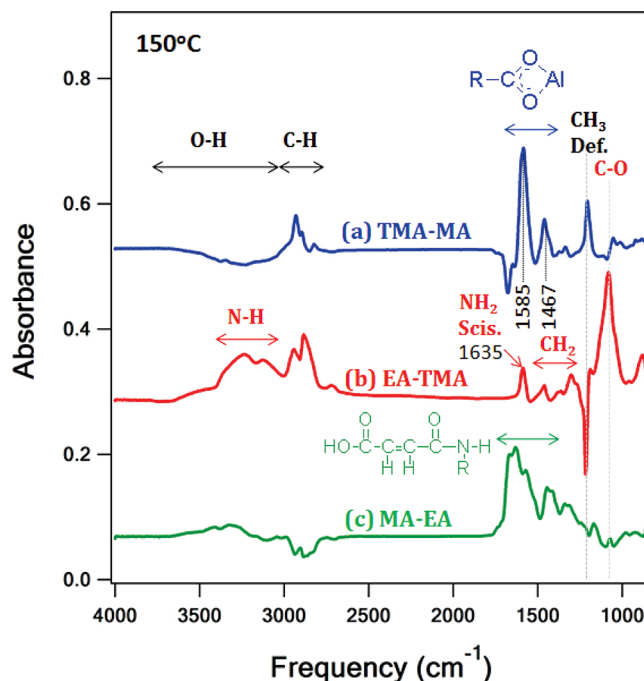
The TMA−MA difference spectrum in Figure 5a is consistent with the reaction of TMA with the carboxylic acid species produced from the previous MA reaction. Positive absorbances are observed for the methyl deformation of $AlCH_3^*$ species and C−H stretching vibrations at 1205 and $2750-3000$ cm^{-1}, respectively. In addition, positive absorbance is observed at 1585 and 1467 cm^{-1}. These absorbances are consistent with the asymmetric $\nu_a(CO_2^-)$ and symmetric $\nu_s(CO_2^-)$ vibrations of an aluminum carboxylate ion (CO_2-Al). The frequency difference of $\Delta = 118$ cm^{-1} between $\nu_a(CO_2^-)$ and $\nu_s(CO_2^-)$ is characteristic of a bidentate complex that typically displays splittings of $\Delta = 50-150$ cm^{-1}.[23] In contrast, unidentate complexes display larger splittings of $\Delta > 200$ cm^{-1} and bridging complexes also display larger splittings of $\Delta = 130-200$ cm^{-1}.[23] Negative absorbance features are monitored in Figure 5a at $1620-1780$ and $3050-3750$ cm^{-1}. These features are consistent with the removal of the carboxylic acid species from the previous MA reaction.

The positive features for the EA−TMA difference spectrum in Figure 5b are consistent with the reaction of EA with $AlCH_3^*$ species from the previous TMA reaction. Positive absorbances are observed for N−H stretching vibrations of the alkoxyamine species at $3160-3420$ cm^{-1}, C−H stretching vibrations of ethylene groups at $2750-3000$ cm^{-1}, NH_2 scissoring modes at 1635 cm^{-1}, and strong C−O stretching vibrations at 1085 cm^{-1}. Small absorbances of CH_2 scissoring, wagging, and twisting modes are also observed at 1390, 1310, and 1270 cm^{-1},

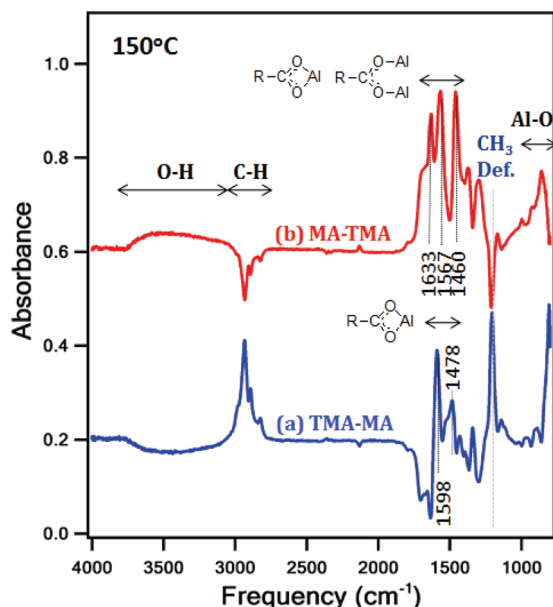(23) Verpoort, F.; Haemers, T.; Roose, P.; Maes, J. P. *Appl. Spectrosc.* **1999**, *53*, 1528.

Figure 6. FTIR difference spectra after TMA and MA exposures during AB alucone MLD with TMA and MA at 150 °C: (a) TMA−MA and (b) MA−TMA. The FTIR spectra after each reactant exposure are referenced with respect to the previous reactant exposure.

respectively. Likewise, the absorbance of Al−O stretching vibrations is measured at 883 cm^{-1}. In addition, a prominent negative absorbance feature is monitored for the loss of the methyl deformation of AlCH$_3$* species at 1210 cm^{-1}.

The positive features for the MA−EA difference spectrum in Figure 5c are in agreement with the ring-opening reaction of MA with the alkoxyamine surface species from the previous EA reaction. The most prominent positive absorbance features are observed at 1490−1740 cm^{-1} for some of the stretching and bending vibrations of the ring-opening product. The characteristic carboxylic acid peak is observed at 1720 cm^{-1}. The carbonyl groups for the carboxylic acid and the amide I are observed at 1668 and 1638 cm^{-1}, respectively. The positive absorbance at 1578 cm^{-1} is assigned to the C=C stretching vibrations present after the ring-opening of MA. The positive absorbance of the C−N stretching vibrations of amide moieties is observed at 1540 cm^{-1}. A small positive absorbance of R=C−H bending modes is also monitored at 1345 cm^{-1}.

A small negative absorbance is observed at 2750−3000 cm^{-1} in Figure 5c that corresponds with the partial loss of C−H stretching vibrations from ethylene species from the previous alkoxyamine surface species. This loss may be caused by the reaction between MA and Al centers on the surface or inside the growing ABC alucone polymer. A substitution reaction could occur where the alkoxyamine may be replaced by the carboxylic acid binding to the Al center. To gain more insight into this possible substitution reaction, a two-step AB MLD reaction was performed using TMA and MA reactants on ZrO$_2$ nanoparticles at 150 °C. Figure 6 displays the FTIR difference spectra after the TMA and MA reactions.

Figure 6a shows the TMA−MA difference spectrum during the two-step AB reaction sequence with TMA and MA. The spectrum in Figure 6a shows positive absorbance features at 1478 and 1598 cm^{-1} that are consistent with an aluminum-coordinated carboxylate ion. The frequency difference of $\Delta = 120$ cm^{-1} between $\nu_a(CO_2^-)$ and $\nu_s(CO_2^-)$ is characteristic of a bidentate complex.[23] Positive absorbance is also observed for Al−O stretching vibrations at 807 cm^{-1}. Tetrahedral Al−O coordination yields stretching vibrations at 750−850 cm^{-1}.[24] In addition, there are positive absorbance features for C−H stretching vibrations at 2750−3000 cm^{-1} and methyl deformations of the AlCH$_3$* species at 1205 cm^{-1}.

The negative absorbance features observed at 1625−1895 and 3050−3770 cm^{-1} in Figure 6a correspond with the loss of carboxylate and hydroxyls on the carboxylic acid surface species, respectively. These negative absorbance features argue that TMA reacts with hydroxyl groups on the carboxylic acid species to form Al−O bonds and bidentate carboxylate bonds. The TMA exposure may also cause restructuring of the carboxylate bonds. This restructuring may lead to a red-shift in the carboxylate frequencies and produce the negative absorbance features at 1625−1895 cm^{-1}.

After the MA reaction, the MA−TMA difference spectrum shown in Figure 6b shows a variety of absorbance features at 1610−1850 cm^{-1}. These absorbance features are assigned to carbonyl stretching vibrations of carboxylic acid, carboxylate ion, and 5-membered cyclic anhydride. The prominent peaks at 1460, 1567, and 1633 cm^{-1} are assigned to bands of bidentate and bridging carboxylate complexes. The frequency differences between $\nu_a(CO_2^-)$ and $\nu_s(CO_2^-)$ are characteristic of a mixture of bidentate complexes with splittings of $\Delta = 50-150$ cm^{-1} and bridging complexes with splittings of $\Delta = 130-200$ cm^{-1}.[23] The cyclic anhydride carbonyl stretching vibrations observed at 1800 cm^{-1} indicates that some MA reactant is absorbed on the polymer surface. There are also positive absorbance features at 3050−3770 cm^{-1} corresponding with O−H stretching vibrations resulting from the ring-opening of MA. Positive absorbance features are also observed at 863 cm^{-1} corresponding with an Al−O stretching vibration.

The AB reaction sequence of TMA and MA could be used to grow another type of AB alucone film. This AB reaction sequence illustrates that MA can bond well with AlCH$_3$* species. Consequently, the MA could react with AlCH$_3$* species during the ABC reaction sequence as observed in Figure 4c. In addition, there may be a probability for MA to displace some alkoxyamine surface species during the ABC reaction sequence because some of the MA reactant may coordinate with Al in the ABC alucone polymer. This displacement would explain the small negative absorbance in the C−H stretching region observed in Figure 5c.

(24) Hubert Joe, I.; Vasudevan, A. K.; Aruldhas, G.; Damodaran, A. D.; Warrier, K. G. K. *J. Solid State Chem.* **1997**, *131*, 181.
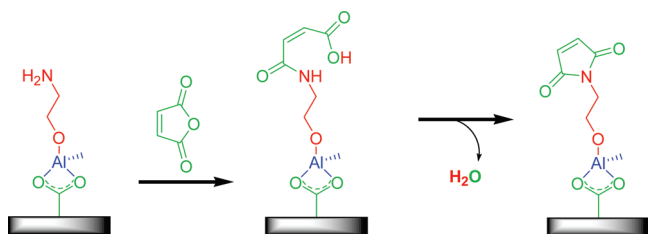
Figure 7. Schematic of possible ring closure to form a maleimide ring after the ring-opening reaction of MA.

After the ring-opening reaction of MA by surface amine species, a 5-member cyclic imide could form resulting from reaction of the carboxylic acid and the secondary amine. This maleimide ring is commonly formed when amine groups are protected using MA or succinic anhydride.[25] A schematic of this ring closure following the ring-opening reaction of MA is shown in Figure 7. The FTIR difference spectra were examined closely to determine if this 5-member cyclic imide is formed after the MA ring-opening reaction or if carboxylic acid species are present on the ABC polymer surface as shown in Figure 1c.

Figure 8 displays an enlargement of the FTIR difference spectra shown in Figure 5c after the MA reaction during the ABC reaction sequence with TMA, EA, and MA. The main absorbances at 1668, 1638, 1578, 1540, 1446, 1345, and 1235 cm^{-1} are identified with the reaction product of MA ring-opening as discussed earlier. In comparison, if a 5-member cyclic imide is formed via the ring-closing reaction shown in Figure 7, the characteristic symmetric and asymmetric stretching vibrations of the maleimide should be observed as absorbance features at ~1720 and ~1790 cm^{-1}.[26] No absorbance is observed at 1790 cm^{-1} in the difference spectrum shown in Figure 8. The absence of this absorbance argues for the MA ring-opening reaction as presented in Figure 1c.

The FTIR spectra of the ABC alucone films were constant in vacuum. Upon exposure to air, changes were observed that were consistent with the ABC alucone films absorbing H_2O. Figure 9 shows a comparison of the absolute FTIR spectra for an initial ABC alucone film grown using 20 ABC MLD cycles at 150 °C and the same ABC alucone film after air exposure for 1 day. After air exposure, there are absorbances from O−H stretching vibrations at 2200−3770 cm^{-1} and absorbed H_2O vibrational modes at 1500−1700 cm^{-1}. Concurrently, the methyl deformation mode of $AlCH_3^*$ species is nearly completely removed from the FTIR spectrum.

Figure 10 shows the FTIR difference spectra that displays the difference between the initial FTIR spectra (Figure 9a) and the FTIR spectra after air exposure for 1 day (Figure 9b). Figure 10 is consistent with the H_2O absorption into the ABC alucone film and the reaction of H_2O with the $AlCH_3^*$ species. The positive absorbance

(25) Larock, R. C. *Comprehensive Organic Transformations*, 2nd ed.; Wiley-VCH: New York, 1999.
(26) Kanoh, S.; Nishimura, T.; Tsuchida, T.; Senda, H.; Motoi, M.; Takani, M.; Matsuura, N. *Macromol. Chem. Phys.* **2001**, *202*, 2489.
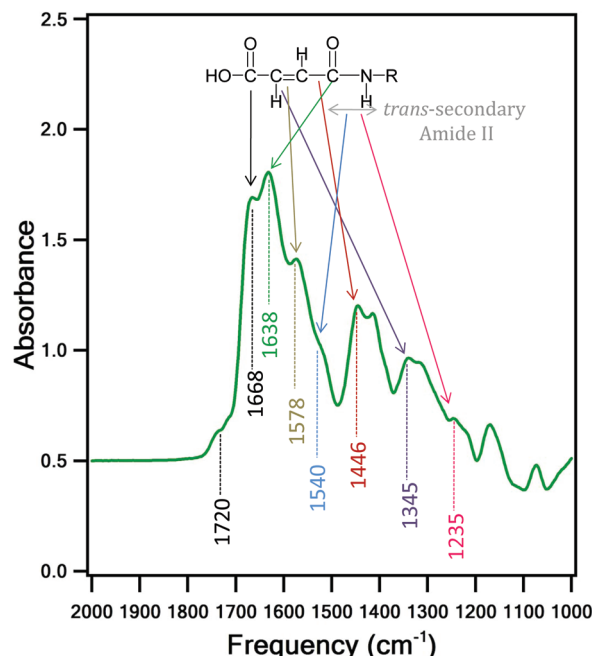
Figure 8. Enlargement of FTIR difference spectra for MA−EA at 1000−2000 cm^{-1} after MA exposure at 150 °C. Vibrational peaks are identified with the product from MA ring-opening.
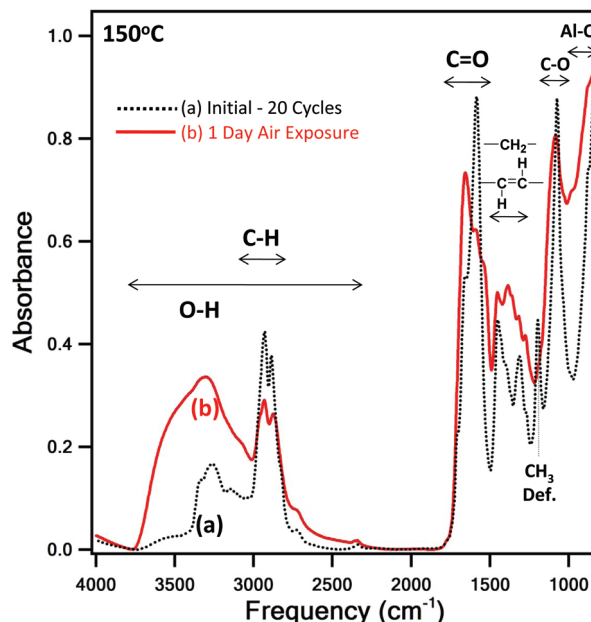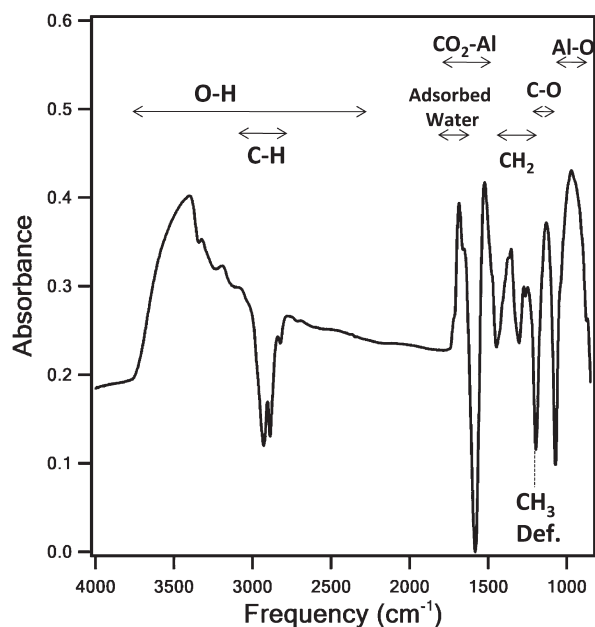

Figure 9. Comparison between absolute FTIR spectra after: (a) 20 MLD cycles at 150 °C and (b) after additional air exposure for 1 day at room temperature.

features correspond with the broad O−H stretching vibrations at 2200−3770 cm^{-1} and the bending modes of absorbed H_2O at 1500−1700 cm^{-1}. The negative absorbance features correspond with the loss of C−H stretching vibrations and the methyl deformation of $AlCH_3^*$ species. Other positive and negative absorbance features are consistent with the slight shifting of C=O modes at 1620−1740 cm^{-1}, C−O modes at 1133 cm^{-1}, and the CH_2 bending, wagging, and twisting modes at 1245−1446 cm^{-1}.

Figure 10. FTIR difference spectrum of the ABC alucone film exposed to air for 1 day at room temperature (Figure 9b) referenced with respect to the ABC alucone film after 20 MLD cycles at 150 °C in vacuum (Figure 9a).

Additional time-dependent FTIR spectra revealed that air exposure is the most critical during the first 10 min after removing the ABC alucone film from vacuum. After the initial spectral evolution during the first 10 min, little change was observed for up to 12 h of air exposure. Likewise, no further changes are observed after multiple days of air exposure. The rapid reaction of the ABC alucone film with H_2O indicates that the ABC alucone film may be useful as a H_2O getter. Gas diffusion barriers are often used to prevent H_2O permeability. An ABC alucone layer in a gas diffusion barrier may serve as an H_2O getter.

B. X-ray Photoelectron Spectroscopy. The composition of the ABC alucone films was investigated using XPS. Figure 11 shows XPS results for an ABC alucone film grown using 120 MLD cycles at 150 °C. The XPS spectrum shows binding energies for C 1s, N 1s, and O 1s at 288.0, 399.5, and 531.3 eV, respectively. According to the XPS database of NIST and earlier literature,[27,28] these observed XPS binding energies are very close to previously reported values for polyamides. XPS binding energies for polyamides for C 1s, N 1s, and O 1s are 288.0, 399.6, and 531.5 eV, respectively. In comparison, the XPS binding energies for polyimides for C 1s, N 1s, and O 1s are 288.9, 400.7, and 532.3 eV, respectively.[29] The XPS results corroborate the MA ring-opening reaction to form the carboxylic acid as shown in Figure 1c.

(27) Beamson, G.; Briggs, D. *High Resolution XPS of Organic Polymers: The Scienta ESCA300 Database*; John Wiley & Sons: New York, 1992.
(28) Wagner, C. D.; Riggs, W. M.; Davis, L. E.; Moulder, J. F.; Muilenberg, G. E. *Handbook of X-ray Photoelectron Spectroscopy*; Perkin-Elmer Corporation: Eden Praire, MN, 1979.
(29) El-Ashgar, N. M.; El-Nahhal, I. M.; Chehimi, M. M.; Connan, C.; Babonneau, F.; Livage, J. *J. Dispersion Sci. Technol.* **2007**, *28*, 445.
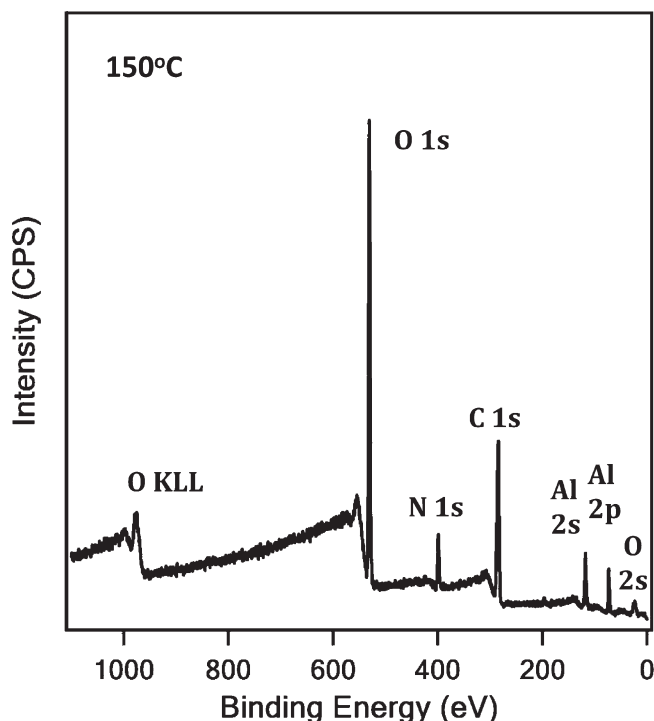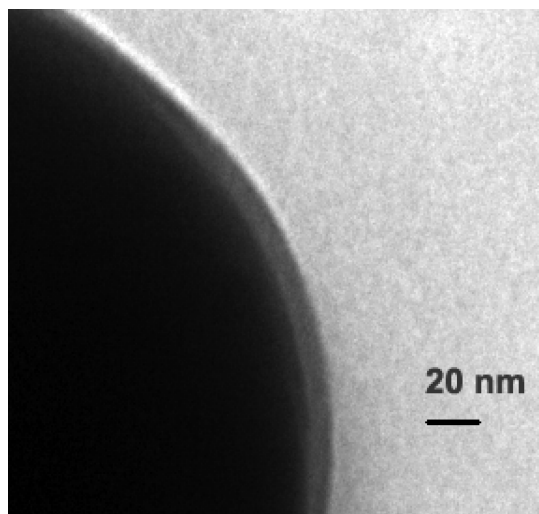
Figure 11. XPS analysis of alucone ABC film after 120 MLD cycles at 150 °C.

Table 2. XPS Analysis of the ABC Alucone Films Grown at Different Temperatures from 90 to 170 °C

rxn temp (°C)	atom %			
	C	N	O	Al
90	46.8	4.5	34.5	14.2
110	46.1	4.6	35.0	14.3
130	44.7	5.2	34.7	15.4
150	44.5	5.6	34.6	15.3
170	39.2	4.2	38.4	18.2

The XPS spectra were consistent with an ABC alucone film atomic composition of 44.5% carbon, 5.6% nitrogen, 34.7% oxygen, and 15.3% aluminum based on the peak areas of each component in Figure 11. The uncertainty of these atomic percentages is <2%. Additional XPS measurements on ABC alucone films grown using 120 MLD cycles at different temperatures from 90 to 170 °C yielded very similar compositions. These XPS results at different reaction temperatures are summarized in Table 2. In contrast, a predicted atomic composition can be calculated for the ABC alucone film based on the reaction mechanism shown in Figure 1. This reaction mechanism corresponds to a polymer formula of $(-AlCH_3-OCH_2CH_2NH-C(O)CHCHCOO-)_n$. The prediction from this formula is 53.8% carbon, 7.7% nitrogen, 30.8% oxygen, and 7.7% aluminum. The ABC alucone MLD film has more aluminum and less carbon and nitrogen than predicted by the expected formula.

The higher aluminum and lower nitrogen atomic percentages can be attributed to some unreacted $AlCH_3*$ species following the EA and MA exposures and to the diffusion of TMA into the ABC alucone films. The diffusion of TMA into and out of the ABC alucone film

Figure 12. TEM image of alucone ABC film on ZrO_2 nanoparticle after 30 MLD cycles at 150 °C.

Figure 13. Film thickness from XRR measurement versus number of MLD cycles for ABC alucone growth at 150 °C.

was measured in quartz crystal microbalance (QCM) studies of ABC alucone MLD.[30] Diffusion of TMA or DEZ into the MLD polymer was also important for the growth mechanism of the alucone[11] and zincone[16] hybrid organic–inorganic MLD polymers. In addition, TMA diffusion into polymers was prominently observed by QCM investigations of Al_2O_3 ALD on polymers.[31] The lower carbon and higher oxygen atomic percentages can also be attributed to water absorption into the alucone film after air exposure. Unreacted $AlCH_3$* species, TMA diffusion, and the partial replacement of alkoxyamine species by MA can explain the higher aluminum and lower nitrogen atomic percentages.

C. Transmission Electron Microscopy and X-ray Reflectivity. The ABC alucone growth per cycle was measured using TEM analysis of the ABC alucone film grown on ZrO_2 nanoparticles at different temperatures. A TEM image of an ABC alucone film after 30 MLD cycles at 150 °C is shown in Figure 12. The ABC alucone film is very conformally deposited on the ZrO_2 nanoparticle. The TEM analysis was performed twice on different samples grown at separate times using 10 MLD cycles. The TEM measurements yielded thicknesses of 48−54 Å. The TEM analysis was also performed twice on different samples grown at separate times after 30 MLD cycles and yielded thicknesses of 138−161 Å. The film thicknesses on the ZrO_2 nanoparticles after 30 MLD cycles are consistent with an ABC alucone growth rate of 4.6−5.4 Å per cycle at 150 °C.

The thickness of ABC alucone films grown at 90−170 °C on Si wafers was also measured using XRR analysis. The ABC reactants were directly deposited on the native SiO_2 layer on the Si wafers. The reactant dosing conditions were the same for the Si wafers and the ZrO_2 nanoparticles. The ABC alucone films appeared clear and transparent on the silicon wafers. The XRR measurements
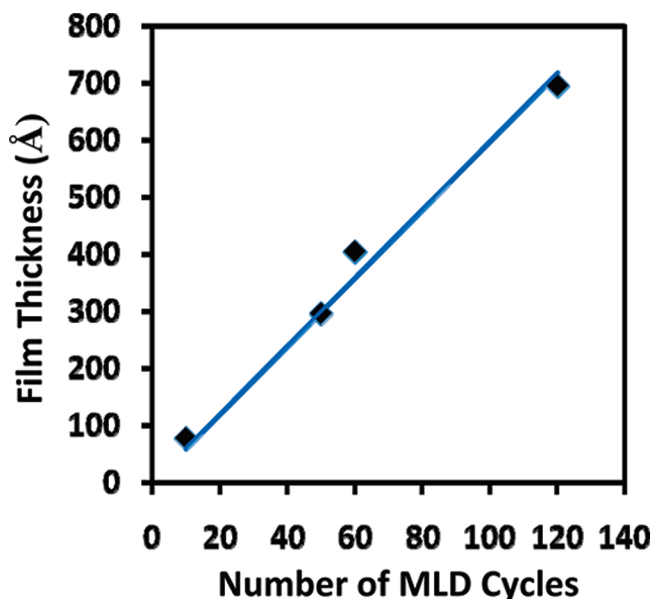
were recorded within 1 h after deposition. Each XRR scan required approximately 40 min. The XRR scans were fit using the REFS data fitting software from Bede Scientific. The film thicknesses after 10, 50, 60, and 120 MLD cycles are shown in Figure 13. The film growth is linear and consistent with a growth rate of 6.0 Å per cycle at 150 °C.

The growth rate of 6.0 Å per cycle at 150 °C on the Si wafer is slightly more than the growth rate of 4.6−5.4 Å per cycle at 150 °C on the ZrO_2 nanoparticles. The different growth rates may be partially explained by the lower gas conductance in the ZrO_2 nanoparticles. The ABC alucone also displayed temperature-dependent growth rates that ranged from 24 Å per cycle at 90 °C to 4.0 Å per cycle at 170 °C. The decrease in the ABC alucone growth per cycle versus temperature can be attributed to more TMA diffusion into the ABC alucone film and less desorption of TMA from the ABC alucone film at lower temperatures.

D. Applications for ABC Alucone Films. Many new applications are possible for these organic–inorganic alucone films grown using the three-step ABC reaction sequence. The hybrid nature of these ABC alucone films gives them a material identity between soft organic polymers and hard inorganic ceramics. In addition, the chemical, mechanical, thermal, and electrical properties should be tunable using different organic reactants with various molecular properties. The wide selection of possible organic reactants should lead to an unprecedented ability to obtain particular material characteristics.

Some mechanical properties of ABC alucone films have recently been measured using nanoindentation studies.[32] The elastic modulus of the ABC alucone film was determined to be 13.2 ± 5.0 GPa.[32] This elastic modulus is

(30) Seghete, D.; Hall, R. A.; George, S. M. unpublished results, **2009**.
(31) Wilson, C. A.; Grubbs, R. K.; George, S. M. *Chem. Mater.* **2005**, *17*, 5625.

(32) Miller, D. C.; Foster, R. R.; Jen, S. H.; Bertrand, J. A.; Seghete, D.; Yoon, B.; Lee, Y. C.; George, S. M.; Dunn, M. L. *Acta Mater.* **2009**, *57*, 5083.

closer to typical values of ~1 GPa for organic polymers than to representative values of ~200−300 GPa for inorganic ceramics. In addition, the Berkovich hardness of the ABC alucone film was 0.27 ± 0.10 GPa.[32] This Berkovich hardness is closer to the hardness values of organic polymers (e.g., 0.1145 ± 0.0036 GPa for poly-epoxypropylcarbazole[33]) than to the hardness values of inorganic ceramics (e.g., 19.52 ± 0.98 GPa for Al_2O_3[34]).

The ABC alucone films may also be useful as flexible interlayers in multilayer films. Multilayer films can be used as gas diffusion barriers on polymers to obtain extremely low gas transmission rates.[35] Multilayer gas diffusion barriers fabricated using only inorganic materials may crack because of film brittleness at larger thicknesses.[36] Multilayer gas diffusion barriers composed of inorganic layers with flexible polymer interlayers may be able to maintain flexibility and also achieve extremely low gas transmission rates.[35] The ABC alucone films can be deposited easily with precise ultrathin thicknesses that may be able to improve the flexibility of multilayer barriers.[37]

The ABC alucone films can also be useful as sacrificial layers to define air gaps for nanofabrication.[38] The organic nature of the ABC alucone films leads to their facile dissolution in HCl solutions.[39] This ease of removal allows the ABC alucone films to be employed as sacrificial layers for the fabrication of nanoelectromechanical systems (NEMS) devices. Recent work has demonstrated the construction of W ALD bridge structures that serve as NEMS switches.[39]

IV. Conclusions

The MLD of a novel hybrid organic−inorganic polymer film was accomplished using trimethylaluminum (TMA), ethanolamine (EA), and maleic anhydride (MA) in a three-step reaction sequence. This process illustrates MLD film growth using a homotrifunctional inorganic precursor (TMA), a heterobifunctional organic reactant (EA), and a ring-opening organic reactant (MA). These reactants should prevent "double" reactions that may limit the number of surface sites and lower the growth per cycle. This ABC alucone polymer should have the approximate formula of $(-AlCH_3-OCH_2CH_2N-H-C(O)CHCHCOO-)_n$.

The film growth and surface chemistry during the ABC alucone MLD was studied by in situ Fourier transform infrared (FTIR) measurements. The FTIR spectra revealed that the TMA, EA, and MA surface reactions were self-limiting. The absorbance of FTIR spectra also progressively increased versus the number of MLD cycles. The TMA−MA, EA−TMA, and MA−EA FTIR difference spectra displayed absorbance changes that supported the reaction mechanism shown in Figure 1. After the ring-opening reaction during MA exposure, a 5-member cyclic imide could form resulting from the reaction of the carboxylic acid and the secondary amine. However, the vibrational spectra did not observe all the characteristic absorbance features consistent with a maleimide ring. Likewise, the XPS binding energies for C 1s, N 1s, and O 1s in the ABC alucone film were more consistent with polyamide than polyimide.

The conformal growth of the alucone ABC film on ZrO_2 nanoparticles was observed by TEM measurements. The TEM analysis determined that the ABC alucone growth rate was consistent with ~5.0 Å per cycle at 150 °C. X-ray reflectivity measurements confirmed linear growth for the alucone ABC films versus number of MLD cycles. The XRR measurements displayed growth rates for ABC alucone films that varied from 24 Å per MLD cycle at 90 °C to 4.0 Å per MLD cycle at 170 °C. The larger diffusion of TMA into the alucone film and slower desorption of TMA out of the alucone film at lower temperatures may explain the temperature dependent growth rates. The ABC alucone films also absorbed H_2O upon exposure to air. The reaction of H_2O with $AlCH_3^*$ species may be useful for the application of ABC alucone films as H_2O getters.

The three-step MLD reaction sequence used to grow the ABC alucone film is very promising. The three-step process offers new possibilities to incorporate a broad set of reactants and to incorporate a wide range of functionalities in the film. The use of organic and inorganic reactants allows the ABC alucone films to have material properties that can be tuned between soft organic polymers and hard inorganic ceramics. These ABC alucone films may be useful for a variety of applications such as flexible films, compliant layers, H_2O getter films, and sacrificial layers.

(33) Palistrant, N. *Mol. J. Phys. Sci.* **2005**, *4*, 468.
(34) Brookes, C. A.; Moxley, B. J. *J. Phys. E: Sci. Instrum.* **1975**, *8*, 456.
(35) Graff, G. L.; Williford, R. E.; Burrows, P. E. *J. Appl. Phys.* **2004**, *96*, 1840.
(36) Dameron, A. A.; Davidson, S. D.; Burton, B. B.; Carcia, P. F.; McLean, R. S.; George, S. M. *J. Phys. Chem. C* **2008**, *112*, 4573.
(37) Cordero, N.; Yoon, J.; Suo, Z. G. *Appl. Phys. Lett.* **2007**, *90*, 111910.
(38) Young, S.; Weston, D.; Dauksher, B.; Mancini, D.; Pacheco, S.; Zurcher, P.; Miller, M. *J. Micromech. Microeng.* **2005**, *15*, 1824.
(39) Seghete, D.; Davidson, B. D.; Hall, R. A.; Chang, Y. J.; Bright, V. M.; George, S. M. *Sens. Actuators A* **2009**, *155*, 8.